# First Principles Calculation of Defect Formation Energies in Sr- and Mg-Doped $LaGaO_3$

**Akihide Kuwabara* and Isao Tanaka**

*Department of Materials Science and Engineering, Kyoto University, Yoshida, Sakyo, Kyoto 606-8501, Japan*

*Received: January 14, 2004; In Final Form: April 9, 2004*

First-principles calculations with projector augmented wave method has been carried out for Sr- and/or Mg-doped rhombohedral $LaGaO_3$. The formation energies of 10 kinds of defects have been systematically computed in consideration of temperature and oxygen partial pressure. $Sr^{2+}$ ion is found to be stable at La site rather than Ga site, whereas $Mg^{2+}$ ion is stable at Ga site. The solution of dopants accompanied with the formation of oxygen vacancies shows the lowest energy at temperatures of 500−1600 K and oxygen partial pressure of $10^{-21}$ to 1 atm. Defects resulting in *n*- or *p*-type conductivity are energetically unfavorable under these conditions. The present theoretical results are consistent with experimental results of doped $LaGaO_3$ in the literature regarding both site preference of dopants and the dependence of ionic conductivity on oxygen partial pressure. Substituting $Sr^{2+}$ and $Mg^{2+}$ ions with the formation of $O^{2-}$ vacancies are confirmed to be predominant defects in temperatures of 500−1600 K and oxygen partial pressures of $10^{-21}$ to 1 atm in *r*-$LaGaO_3$ by means of first principles calculation.

## 1. Introduction

Fast oxygen ion conductors are important materials because of their prospective application in oxygen pump, oxygen sensor, and solid oxide fuel cell (SOFC). It has been widely noted that many perovskite-type oxides exhibit high diffusivity of oxygen ions.[1−4] $LaGaO_3$ shows an orthorhombic structure (*Pnma*; *o*-$LaGaO_3$) at room temperatures.[5,6] *o*-$LaGaO_3$ transforms to a rhombohedral structure (*R*3*c*; *r*-$LaGaO_3$) at temperatures higher than about 150 °C.[5,6] Recently, Sr and Mg co-doped $LaGaO_3$ (LSGM) has attracted extensive attention and is expected to be one of the best candidates for solid electrolyte in SOFC, because the oxygen ionic conductivity of LSGM is higher than that of a standard oxygen ionic conductor, namely yttria-stabilized zirconia.[7] LSGM also has a superior characteristic showing stable ionic conductivity in a wide range of oxygen partial pressures.[7−10]

For designing ionic conductive materials, it is necessary to comprehend defect chemistry, because ionic conductivity takes place via lattice defects. The formation energy of a lattice defect is one of the major factors that determine oxygen ionic conductivity. Many computational simulations on the basis of lattice statics and molecular dynamics using empirical interatomic potentials have been conducted to investigate the energetics of intrinsic defects, the solution state of foreign dopant, and the migration of cation and $O^{2-}$ ion in doped $LaGaO_3$.[11−14] These previous works were successful in reproducing some trends found by experiments. However, first-principles calculations are necessary to understand the electronic mechanism behind the high conductivity. Calculations without empirical parameters are mandatory to design new materials. Despite the importance of LSGM, no first principles results of this system have thus far been available.

In the present paper, we have concentrated on defect chemistry in *r*-$LaGaO_3$ and computed defect formation energies as a function of temperature and oxygen partial pressure. First principles calculation was combined with thermodynamical theory. We have paid special attention to the solution states of $Sr^{2+}$ and $Mg^{2+}$ ions those were typical dopants for $LaGaO_3$, because *p*- and *n*-type conductivity should be avoided in ionic conductors.

## 2. Calculation Methodology

We employed VASP code,[15,16] which is based on density functional theory (DFT). The exchange and correlation functional was given by the generalized gradient approximation (GGA) as proposed by Perdew and Wang.[17] Electron−ion interaction was represented by the projector augmented wave (PAW) method[18,19] with plane waves up to an energy of 600 eV. The configurations of valence electrons were $5s^2\ 5p^6\ 6s^2\ 5d^1\ 4f^0$ for La, $3d^{10}\ 4s^2\ 4p^1$ for Ga, $4s^2\ 4p^6\ 5s^2$ for Sr, $2p^6\ 3s^2$ for Mg, and $2s^2\ 2p^4$ for O. Before analyses of doped $LaGaO_3$, preliminary calculations for perfect and undoped $LaGaO_3$ were performed. Three polymorphs, orthorhombic (*o*-$LaGaO_3$), rhombohedral (*r*-$LaGaO_3$), and cubic (*c*-$LaGaO_3$) structures were considered in the present study. The **k**-point meshes of Brillouin zone sampling in primitive cells, based on the Monkhorst-Pack scheme,[20] were $4 \times 3 \times 4$ for *o*-$LaGaO_3$ (8 irreducible points), $5 \times 5 \times 5$ for *r*-$LaGaO_3$ (44 irreducible points), and $7 \times 7 \times 7$ for *c*-$LaGaO_3$ (20 irreducible points) in order to obtain absolute energy convergence $\leq$ 1 meV/atom. Lattice constants and internal positions in the primitive cell of each crystal structure were fully optimized under the condition of residual force $\leq$ 0.02 eV/Å.

A supercell including a point defect was constructed using the fully optimized primitive cell of *r*-$LaGaO_3$ structure. The supercell includes 80 atoms, and its size is $11.05 \times 11.05 \times 11.05$ Å$^3$ with angles of 60.87° formed by lattice vectors. Cutoff energy was set to be the same as that of perfect crystals. The **k**-meshs of $2 \times 2 \times 2$ were chosen for attaining absolute energy convergence $\leq$ 1 meV/atom. Structural relaxation was limited within a spherical region with a radius of 3.2 Å from a defect site.

10.1021/jp049808m CCC: $27.50 © 2004 American Chemical Society
Published on Web 05/28/2004

The formation energy of a point defect ($E_{defect}$) was evaluated using the following equation:[21]

$$E_{defect}(q) = E_{supercell}^{t}(q) - N_{La}\mu_{La} - N_{Ga}\mu_{Ga} - N_{O}\mu_{O} - N_{d}\mu_{d} + qE_{f} \quad (1)$$

where $E_{supercell}^{t}(q)$ is the calculated total energy of a supercell containing a defect with a charged state of $q$; $N_{La}$, $N_{Ga}$, $N_{O}$, and $N_{d}$ correspond to the number of La, Ga, O, and dopant atoms in the supercell, respectively; $\mu_{La}$, $\mu_{Ga}$, $\mu_{O}$, and $\mu_{d}$ represent the chemical potential of La, Ga, O, and dopant atoms, respectively. $E_f$ is the Fermi energy, namely, the chemical potential of electrons. The charges of the supercell were neutralized by a standard method using a jellium background. Energy shifts associated with jellium neutralization were estimated by total energy difference between neutral and charged supercells of a perfect crystal. For example, electrons were removed from the valence-band maximum of a positively charged perfect crystal, and jellium neutralization was included. Correcting this energy shift should correspond to setting the energy of valence-band top ($E_{VBT}$) to be reference for the Fermi energy. The total energy of a supercell with a positively charged defect, $E_{supercell}^{t}(q)$ for $q > 0$, was evaluated with this reference. The energy of a negatively charged system was obtained by the same manner. In this case, the energy of conduction-band bottom ($E_{CBB}$) was used as reference for the Fermi energy.

Several kinds of defects related to electrical conductivity were taken into account in doped-$LaGaO_3$ systems. For Sr-doped $r$-$LaGaO_3$, they were $Sr'_M + h^{\bullet}$ (M = La, Ga), $Sr'_M + 1/2V_O^{\bullet\bullet}$, $V_O^{\bullet} + e'$ and $V_O^{\bullet\bullet} + 2e'$ according to the Kröger-Vink notation. $Sr'_M + h^{\bullet}$ corresponds to a case showing $p$-type conductivity. This model was examined using a negatively charged supercell, i.e., $Sr_M(-1)$, and the energy of a hole was considered by $E_f$ as given in eq 1. An oxygen vacancy is associated with two negatively charged Sr in the model of $Sr'_M + 1/2V_O^{\bullet\bullet}$. In this case, oxygen ionic conductivity is expected because of the presence of oxygen vacancies. The solution energy of this model can be computed using a large supercell with two substitutional $Sr^{2+}$ ions and an $O^{2-}$ vacancy. However, such calculation for multiple defects requires a large supercell, which is computationally demanding. In the present study, we have chosen an alternative way by calculations of two independent charged supercells, i.e., $Sr_M(-1)$ and $V_O(+2)$ for convenience. Two total energies were summed following the equation of $Sr_M(-1) + 1/2V_O(+2)$. $V_O^{\bullet} + e'$ and $V_O^{\bullet\bullet} + 2e'$ result in $n$-type conductivity. The formation energies of these models were evaluated using charged supercells of $V_O(+1)$ and $V_O(+2)$ under the condition that $E_f$ in eq 1 was taken equal to $E_{CBB}$. This procedure means that the formation of electron in conduction band was allowed for. Energy difference between $E_{CBB}$ and $E_{VBT}$, namely, band-gap ($E_g$), can be measured as $\{E(+1) - E(0)\} - \{E(0) - E(-1)\}$, where $E(N)$ indicates the total energy of a perfect lattice supercell with additional $N$ electrons.

As indicated in eq 1, the defect formation energy depends on the chemical potential of each element. The chemical potential was determined under the condition of phase coexistence. Figure 1 shows schematic phase diagrams in $La_2O_3$−$Ga_2O_3$−SrO and $La_2O_3$−$Ga_2O_3$−MgO pseudo-ternary systems on the basis of experimental phase diagrams.[22]

Six thermodynamical conditions are indicated by arrows in this Figure. For example, $r$-$LaGaO_3$ coexists with $La_4Ga_2O_9$ and $LaSrGaO_4$ at point A. Assumed that thermodynamical equilibrium is achieved, chemical potentials of constituent elements are equal among coexisting phases. Therefore, chemical potentials, $\mu_{La}$, $\mu_{Ga}$, $\mu_{Sr}$, and $\mu_{O}$, are correlated according to the following equations at point A

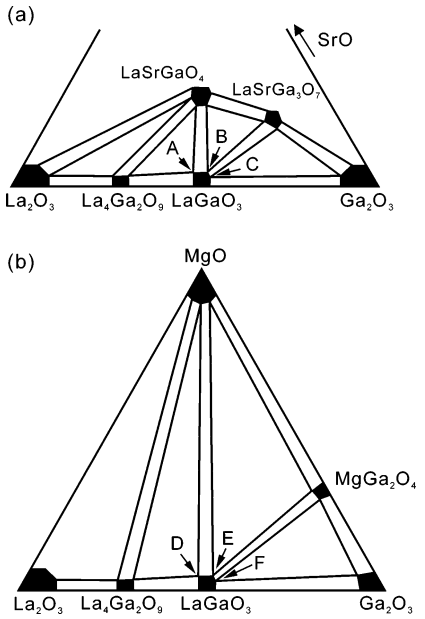


**Figure 1.** Schematic phase diagrams of (a) $La_2O_3$−$Ga_2O_3$−SrO and (b) $La_2O_3$−$Ga_2O_3$−MgO pseudo-ternary systems.

$$\mu_{La} + \mu_{Ga} + 3\mu_{O} = \mu_{r\text{-}LaGaO_3(bulk)} \quad (2)$$

$$4\mu_{La} + 2\mu_{Ga} + 9\mu_{O} = \mu_{La_4Ga_2O_9(bulk)} \quad (3)$$

and

$$\mu_{La} + \mu_{Sr} + \mu_{Ga} + 4\mu_{O} = \mu_{LaSrGaO_4(bulk)} \quad (4)$$

where $\mu_{r\text{-}LaGaO_3(bulk)}$, $\mu_{r\text{-}La_4Ga_2O_9(bulk)}$, and $\mu_{LaSrGaO_4(bulk)}$ are the total energies per molecule of perfect $r$-$LaGaO_3$, $La_4Ga_2O_9$, and $LaSrGaO_4$ bulks, respectively. These phases were assumed to coexist with $O_2$ gas phase. Therefore, the chemical potential of oxygen is uniquely determined as

$$\mu_{O} = \frac{1}{2}\mu_{O_2(gas)} \quad (5)$$

where $\mu_{O_2(gas)}$ is the total energy per molecule of gaseous $O_2$. The chemical potentials of cations at point A were obtained by calculating the total energies of the coexisting four phases and solving eqs 2−5 simultaneously. The chemical potentials at points B to F were acquired by a manner similar to the point A.

Calculations applied to metallic La ($P6_3/mmc$), metallic Ga ($Cmca$), intermetallic LaGa ($Cmcm$), $La_2O_3$ ($P\bar{3}m1$), $La_4Ga_2O_9$ ($P2_1/c$), $Ga_2O_3$ ($C2/m$), $LaSrGaO_4$ ($I4/mmm$), $LaSrGa_3O_7$ ($P\bar{4}2_1m$), and $MgGa_2O_4$ ($Fd\bar{3}m$) employed **k**-meshes based on the Monkhorst-Pack scheme of 17 × 17 × 5 (99 irreducible points), 15 × 15 × 13 (448 irreducible points), 10 × 8 × 10 (180 irreducible points), 5 × 5 × 3 (12 irreducible points), 2 × 2 × 2 (2 irreducible points), 6 × 12 × 4 (84 irreducible points), 6 × 6 × 6 (28 irreducible points), 3 × 3 × 3 (10 irreducible points), and 5 × 5 × 5 (10 irreducible points), respectively. In both $LaSrGaO_4$ and $LaSrGa_3O_7$, [La and Sr have been reported to randomly occupy a single crystallographic site with the ratio of 1:1.[23,24] We calculated the energies of primitive cells with all possible relative positions between La and Sr. The primitive cell with the lowest energy was then adopted as the reference

**TABLE 1: Optimized Lattice Constant and Formation Enthalpy per Formula Unit of Compounds in $La_2O_3-Ga_2O_3$ System**

| | | lattice constant/Å | | $\Delta_f E$/eV·f.u.$^{-1}$ | $\Delta_f H°$/eV·f.u.$^{-1}$ |
|---|---|---|---|---|---|
| | | present study | exp | present study | exp[a] |
| *c*-$LaGaO_3$ | *a* | 3.91 | | −13.50 | |
| *r*-$LaGaO_3$ | *a* | 5.60 | 5.54[b] | −13.78 | |
| | *c* | 13.44 | 13.40[b] | | |
| *o*-$LaGaO_3$ | *a* | 5.58 | 5.49[b] | −13.81 | −15.29 ± 0.16 |
| | *b* | 7.87 | 7.77[b] | | |
| | *c* | 5.56 | 5.52[b] | | |
| $La_4Ga_2O_9$ | *a* | 8.01 | 7.97[c] | −46.08 | −49.16 ± 0.34 |
| | *b* | 11.26 | 11.20[c] | | |
| | *c* | 11.71 | 11.62[c] | | |
| | *β* | 109.37 | 109.46[c] | | |
| $La_2O_3$ | *a* | 3.94 | 3.94[d] | −17.62 | −18.60 ± 0.02 |
| | *c* | 6.19 | 6.13[d] | | |
| $Ga_2O_3$ | *a* | 12.42 | 12.21[e] | −9.58 | −11.31 ± 0.03 |
| | *b* | 3.08 | 3.04[e] | | |
| | *c* | 5.87 | 5.80[e] | | |
| | *β* | 103.71 | 103.83[e] | | |

[a] Ref 27. [b] Ref 6. [c] Ref 25. [d] Ref 26. [e] Ref 28.

**TABLE 2: Formation Enthalpy per Formula Unit of $LaGaO_3$ and $La_4Ga_2O_9$ from Binary Oxides**

| | $\Delta_f E_{oxide}$/eV·f.u.$^{-1}$ | | $\Delta_f H_{oxide}$/eV·f.u.$^{-1}$ |
|---|---|---|---|
| | present study | calc[a] | exp[b,c] |
| *c*-$LaGaO_3$ | 0.11 | | |
| *r*-$LaGaO_3$ | −0.17 | | |
| *o*-$LaGaO_3$ | −0.20 | −0.93 | −0.33 ± 0.17[b] |
| | | | −0.53 ± 0.03[c] |
| $La_4Ga_2O_9$ | −1.25 | −1.58 | −0.65 ± 0.33[b] |

[a] Ref 13. [b] Ref 28. [c] Ref 29.

structure.] The convergence of absolute energy was found to be ≤ 1 meV/atom. For the calculation of oxygen gas phase, an $O_2$ molecule was put into a vacuum cell whose dimensions were identical to that of the supercell of *r*-$LaGaO_3$. The **k**-mesh in a calculation for an $O_2$ molecule was 2 × 2 × 2 (4 irreducible points). Spin-polarization was taken into account for the calculation of $O_2$.

## 3. Results and Discussion

**3.1. $LaGaO_3$ and Other Compounds in the $La_2O_3-Ga_2O_3$ System.** Table 1 shows the optimized lattice constants and the formation energies ($\Delta_f E$) of $LaGaO_3$ and other compounds in the $La_2O_3-Ga_2O_3$ system. Geometrical parameters are good agreement with experimental values within the accuracy of DFT calculations. Theoretical $\Delta_f E$ are underestimated compared to the experimental $\Delta_f H°$ of compounds, which is also typical in this kind of calculation. However, relative stability among polymorphs should be more reliable. Table 1 indicates that the stability of $LaGaO_3$ polymorphs changes as *o*-$LaGaO_3$ > *r*-$LaGaO_3$ > *c*-$LaGaO_3$. The formation energies of $LaGaO_3$ and $La_4Ga_2O_9$ from $La_2O_3$ and $Ga_2O_3$ as reference compounds ($\Delta_f E_{oxide}$) are also evaluated as shown in Table 2. The $\Delta_f E_{oxide}$ of *c*-$LaGaO_3$ is positive, whereas those of the other two phases are negative. The $\Delta_f E_{oxide}$ of *o*-$LaGaO_3$ and $La_4Ga_2O_9$ satisfactorily agree with experimental $\Delta_f H_{oxide}$. To our knowledge, our work is the first calculation, which can reproduce the energetical hierarchy of $LaGaO_3$ polymorphs without any fitting-parameters.

**3.2. Defect Formation Energy in Doped-$LaGaO_3$.** The electrical conductivity of solid electrolytes should take place entirely via ionic conduction. In other words, their transference number for an ionic species should be unity, and that for electrons or holes should be suppressed as small as possible.

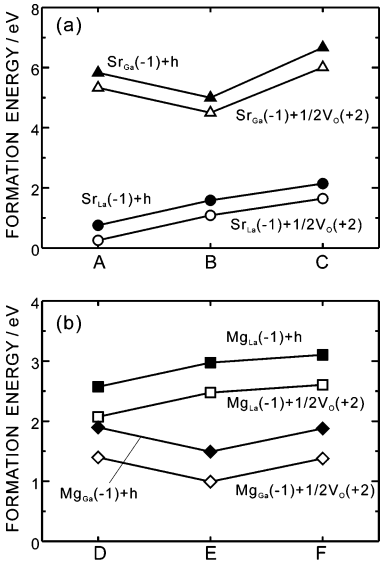


**Figure 2.** Formation energy of substitutional $Sr^{2+}$ and $Mg^{2+}$ ions with oxygen vacancies ($V_O(+2)$) or holes (h) in *r*-$LaGaO_3$ at a temperature of 1300 K and an oxygen partial pressure of 1 atm. Subscript means a substituting cation site. A−F correspond to the phase equilibrium conditions as shown in Figure 1.

Generally, hole conduction in an oxidizing ambience and electronic conduction in a reducing ambience need to be avoided in oxide systems. For example, in Sr-doped $LaGaO_3$, *p*-type conductivity appears when the following reaction takes place in an oxidization atmosphere

$$Sr'_M + 1/2V_O^{\bullet\bullet} + 1/2O_2(g) \rightarrow Sr'_M + h^{\bullet} + O_O^{\times}$$

*n*-type conductivity in a reduction atmosphere occurs by the following reaction:

$$O_O^{\times} \rightarrow V_O^{\bullet\bullet} + 2e' + 1/2O_2(g)$$

We took account of the influence of oxygen partial pressure and temperature in our evaluation of $E_{defect}$. Assuming that $O_2$ is an ideal gas, the chemical potential of oxygen at a partial pressure of $p$ and a temperature of $T$ is described as

$$\mu_O = \frac{1}{2}\left\{\mu_{O_2}(T,p°) + kT\ln\frac{p}{p°}\right\} \quad (6)$$

where $p°$ is the partial pressure of $O_2$ at the standard state, i.e., 1 atm, and $\mu_{O_2}(T,p°)$ corresponds to a total energy per $O_2$ molecule at a temperature of $T$ and partial pressure of $p°$. $\mu_{O_2}(T,p°)$ can be divided into enthalpy ($H$) and entropy ($S$) as

$$\mu_{O_2}(T,p°) = \{H_{O_2}(T,p°) - H_{O_2}(0,p°)\} - T\cdot S_{O_2}(T,p°) + H_{O_2}(0,p°) \quad (7)$$

In the present study, the temperature dependence of $H$ and $S$ in eq 7 was obtained from thermochemical tables.[30] Assuming that the calculated total energy of an $O_2$ molecule corresponds to $H_{O_2}(0, p°)$, the chemical potential of oxygen can be obtained at given $T$ and $p$ using eqs 6 and 7.

Figure 2 shows the formation energies of substitutional $Sr^{2+}$ and $Mg^{2+}$ ions in *r*-$LaGaO_3$ at $T$ = 1300 K and $p$ = 1 atm under the phase equilibrium conditions denoted by A to F as defined in Figure 1.

As indicated in this figure, $Sr^{2+}$ ions have the lowest solution energy when they are substituted for $La^{3+}$ ions with the

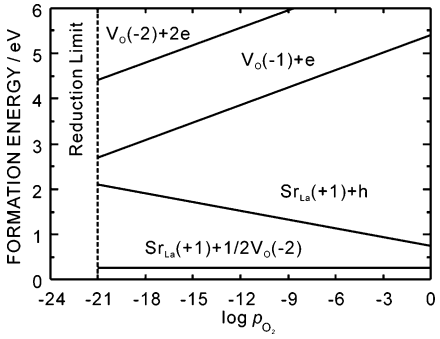


**Figure 3.** Relationship between formation energy of defect and oxygen partial pressure in Sr-doped *r*-$LaGaO_3$ at 1300K under the phase equilibrium condition of $LaGaO_3-LaSrGaO_4-La_4Ga_2O_9-O_2$.

formation of $O^{2-}$ vacancies. Substitution for $Ga^{3+}$ ions needs much higher energy. This must be ascribed to the fact that the ionic radius of $Sr^{2+}$ (1.18 Å, Coordination Number (CN) = 6) is close to that of $La^{3+}$ (1.03 Å, CN = 6) rather than that of $Ga^{3+}$ (0.62 Å, CN = 6).[31] On the other hands, $Mg^{2+}$ ions are likely to be located at Ga site with $O^{2-}$ vacancies. This can be also explained by the small ionic size of $Mg^{2+}$ (0.57 Å, CN = 6).[31] The site preferences of Sr and Mg ions are in good agreement with previous experiments.[6] Sr-doped $LaGaO_3$ is known to act as good oxygen ion conductor at a temperature of 1300 K and an oxygen partial pressure of 1 atm. Therefore, these dopants are presumed to dissolve into $LaGaO_3$ with the formation of $O^{2-}$ vacancies. This tendency is well reproduced by the calculation.

Figure 3 shows the dependence of defect formation energies on oxygen partial pressure in Sr-doped $LaGaO_3$ at 1300K under the equilibrium condition of point A. Considering the coexistence of $LaGaO_3$, intermetallic LaGa, and gaseous $O_2$ phases as a reduction limit, oxygen partial pressure in a reducing atmosphere is limited to $10^{-21}$ atm at 1300 K. These results show that $Sr'_{La} + 1/2V_O^{\bullet\bullet}$ is the dominant defect rather than $Sr'_{La} + h^{\bullet}$, $V_O^{\bullet} + e'$, and $V_O^{\bullet\bullet} + 2e'$ in the whole range of oxygen partial pressures from 1 atm to the reduction limit at 1300 K.

Panels a and b of Figure 4 are plots of defect formation energy against temperature at oxygen partial pressures of 1 and $10^{-21}$ atm, respectively. A condition of phase coexistence is the same as Figure. 3. When the oxygen partial pressure is 1 atm, substituting $Sr^{2+}$ ions accompanied with $O^{2-}$ vacancies is more stable than those with holes at temperatures higher than 500 K. In reducing ambience, the formation energy of $Sr'_{La} + 1/2V_O^{\bullet\bullet}$ is lower than those of $V_O^{\bullet} + e'$, $V_O^{\bullet\bullet} + 2e'$ and $Sr'_{La} + h^{\bullet}$ in the temperature range of 200−2000 K. These calculations for Sr-doped *r*-$LaGaO_3$ have revealed that substituting $Sr^{2+}$ ions with $O^{2-}$ vacancies are predominant defects in a wide range of temperature and oxygen partial pressure.

Majewski et al.[22] have reported on four kinds of four solid-phase regions containing $LaGaO_3$ in LSGM systems; (i) $LaGaO_3-LaSrGaO_4-LaSrGa_3O_7-MgO$ (ii) $LaGaO_3-LaSrGaO_4-La_4Ga_2O_9-MgO$, (iii) $LaGaO_3-LaSrGa_3O_7-MgGa_2O_4-MgO$, and (iv) $LaGaO_3-LaSrGa_3O_7-MgGa_2O_4-Ga_2O_3$. The chemical potentials of constituent elements were calculated in consideration of phase equilibrium among the four solid phases and $O_2$ gas phase. Defect formation energies are plotted as a function of oxygen partial pressure at 1300 K under the phase equilibrium conditions of (i) and (ii) in panels a and b of Figure 5, respectively. The solution energies of $Sr^{2+}$ and $Mg^{2+}$ ions depend on the phase equilibrium condition. However, the substitutional dopants with $O^{2-}$ vacancies are energetically

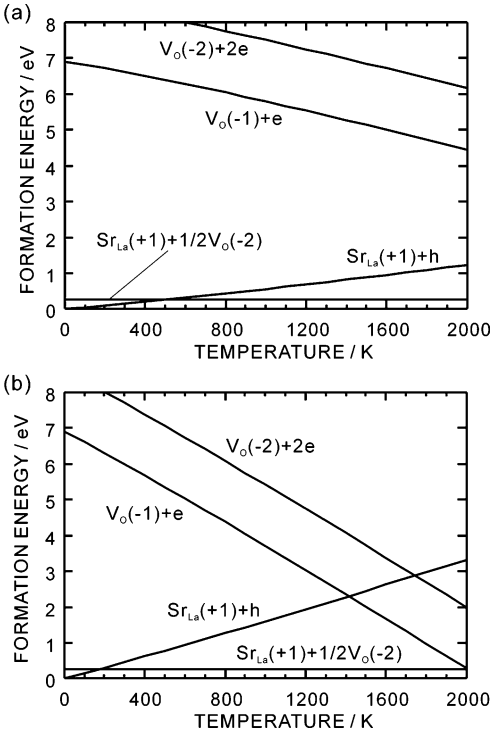


**Figure 4.** Relationship between formation energy of defect and temperature in Sr-doped *r*-$LaGaO_3$ under the thermodynamical condition of $LaGaO_3-LaSrGaO_4-La_4Ga_2O_9-O_2$ at oxygen partial pressures of (a) 1 atm and (b) $10^{-21}$atm.

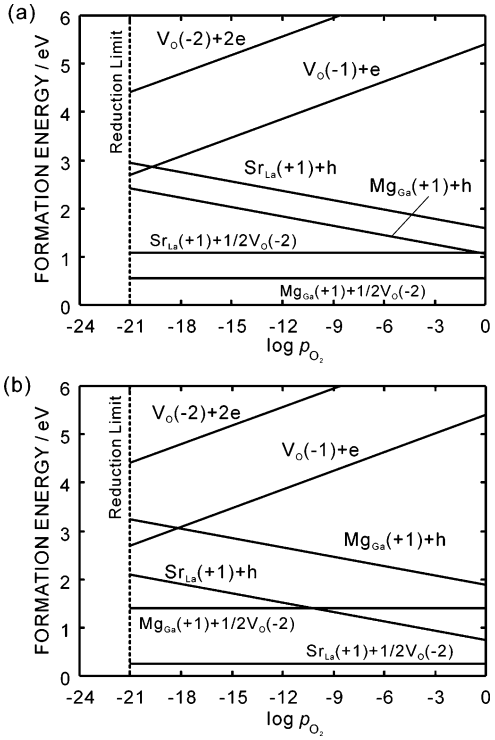


**Figure 5.** Relationship between formation energy of defect and oxygen partial pressure in Sr- and Mg-doped *r*-$LaGaO_3$ under the phase equilibrium conditions of (a) $LaGaO_3-LaSrGaO_4-LaSrGa_3O_7-MgO-O_2$ and (b) $LaGaO_3-LaSrGaO_4-La_4Ga_2O_9-MgO-O_2$ at 1300 K.

favorable in comparison with other defects leading to *p*- or *n*-type conductivity over the whole range of oxygen partial pressures from 1 atm to the reduction limit. Similar tendencies were also observed under the equilibrium conditions of (iii) and

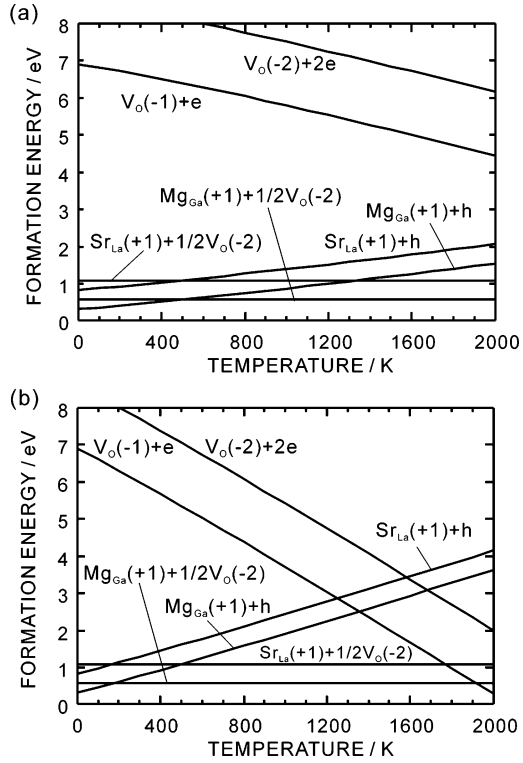


**Figure 6.** Relationship between formation energy of defect and temperature in Sr- and Mg-doped *r*-$LaGaO_3$ under the phase equilibrium condition of $LaGaO_3-LaSrGaO_4-LaSrGa_3O_7-MgO-O_2$ at oxygen partial pressures of (a) 1 and (b) $10^{-21}$ atm.

**TABLE 3: Temperature Range where Substitutional Dopants with $O^{2-}$ Vacancies Has the Lowest Formation Energy at Oxygen Partial Pressures from $10^{-21}$ to 1 Atm in Sr- and Mg-Doped *r*-$LaGaO_3$**

| phase equilibrium condition | temperature range |
|---|---|
| $LaGaO_3-LaSrGaO_4-LaSrGa_3O_7-MgO$ | 500−1700 K |
| $LaGaO_3-LaSrGaO_4-La_4Ga_2O_9-MgO$ | 500−1600 K |
| $LaGaO_3-LaSrGa_3O_7-MgGa_2O_4-MgO$ | 500−1600 K |
| $LaGaO_3-LaSrGa_3O_7-MgGa_2O_4-Ga_2O_3$ | 500−1600 K |

(iv). LSGM maintain dominant ionic conductivity against the variation of oxygen partial pressures at 1300 K.

Panels a and b of Figure 6 are plots of formation energy against temperature under the condition of (i) at oxygen partial pressures of 1 and $10^{-21}$ atm, respectively. In both oxidizing and reducing ambience, the formation energies of $Sr'_{La} + 1/2V_O^{\bullet\bullet}$ and $Mg'_{Ga} + 1/2V_O^{\bullet\bullet}$ are more stable than the other defects in a temperature range of 500−1700 K. Regardless of the phase equilibrium conditions, substituting dopants with $O^{2-}$ vacancies has the lowest formation energy at oxygen partial pressures of $10^{-21}$ to 1 atm and temperatures of 500−1600 K as shown in Table 3. Transference number for ionic conductivity cannot be evaluated only from the formation energies of charge carriers. However, our calculations are in agreement with the experimental result of ionic conductive domain expressed by a function of oxygen partial pressure and temperature in LSGM.[8−10]

## 4. Conclusion

Defect formation energies in Sr- and/or Mg-doped $LaGaO_3$ were evaluated by a first principles calculation, VASP code, combined with thermodynamics theory. $Sr^{2+}$ and $Mg^{2+}$ ions are likely to substitute for $La^{3+}$ and $Ga^{3+}$ ones, respectively. Substitutional $Sr^{2+}$ and $Mg^{2+}$ ions accompanied with $O^{2-}$ vacancies are dominant defects in the entire range of oxygen partial pressures from $10^{-21}$ to 1 atm and of temperatures from 500 to 1600 K. The present study explains why LSGM exhibits stable ionic conductivity in wide ranges of temperature and oxygen partial pressure as experimentally found in refs 8−10. It is confirmed that the combination of modern ab initio calculations and thermodynamics theory are powerful for the field of ionic conductors. Rational material design can be contemplated through theoretical works.

**Acknowledgment.** This work was supported by four projects from the Ministry of Education, Culture, Sports, Science, and Technology of Japan. They are a Grant-in-Aid for Scientific Research on Priority Areas (No. 751), a Grant-in-Aid for Japan Society for the Promotion of Science Fellows (14-08214), the Computational Materials Science Project in Kyoto University, and the 21st century COE program.

## References and Notes

(1) Cook, R. L.; Sammells, A. F. *Solid State Ionics* **1991**, *45*, 311−321.
(2) Mizusaki, J. *Solid State Ionics* **1992**, *52*, 79−91.
(3) Mizusaki, J.; Yasuda, I.; Shimoyama, J.; Yamauchi, S.; Fueki, K. *J. Electrochem. Soc.* **1993**, *140*, 467−471.
(4) Kendall, K. R.; Navas, C.; Thomas, J. K.; Loye, H.-C. *Solid State Ionics* **1995**, *82*, 215−223.
(5) Marti, W.; Fisher, P.; Altorfer, F.; Scheel, H. J.; Tadin, M. *J. Phys. Condens. Matter* **1994**, *6*, 127−135.
(6) Slater, P. R.; Irvine, J. T. S.; Ishihara, T.; Takita, Y. *J. Solid State Chem.* **1998**, *139*, 135−143.
(7) Ishihara, T.; Matsuda, H.; Takita, Y. *J. Am. Chem. Soc.* **1994**, *116*, 3801−3803.
(8) Ishihara, T.; Kilner, J. A.; Honda, M.; Takita, Y. *J. Am. Chem. Soc.* **1997**, *119*, 2747−2748.
(9) Stevenson, J. W.; Armstrong, T. R.; McCready, D. E.; Pederson, L. R.; Weber, W. J. *J. Electrochem. Soc.* **1997**, *144*, 3613−3620.
(10) Kim, J.-H.; Yoo, H.-I. *Solid State Ionics* **2001**, *140*, 105−113.
(11) Khan, M. S.; Islam, M. S.; Bates, D. R. *J. Phys. Chem. B* **1998**, *102*, 3099−3104.
(12) Islam, M. S. *J. Mater. Chem.* **2000**, *10*, 1027−1038.
(13) De Souza, R. A.; Maier, J. *Phys. Chem. Chem. Phys.* **2003**, *5*, 740−748.
(14) Yamamura, Y.; Ihara, C.; Kawasaki, S.; Sakai, H.; Suzuki, K.; Takami, S.; Kubo, M.; Miyamoto, A. *Solid State Ionics* **2003**, *160*, 93−101.
(15) Kresse, G.; Furthmüller, J. *Phys. Rev. B* **1996**, *54*, 11169−11186.
(16) Kresse, G.; Furthmüller, J. *Comput. Mater. Sci.* **1996**, *6*, 15−50.
(17) Perdew, J. P.; Wang, Y. *Phys. Rev. B* **1986**, *33*, 8800−8802.
(18) Blöchl, P. E. *Phys. Rev. B* **1994**, *50*, 17953−17978.
(19) Kresse, G.; Joubert, D. *Phys. Rev. B* **1999**, *59*, 1758−1775.
(20) Monkhorst, H. J.; Pack, J. D. *Phys. Rev. B* **1976**, *13*, 5188−5192.
(21) Zhang, S. B.; Northrup, J. E. *Phys. Rev. Lett.* **1991**, *67*, 2339−2342.
(22) Majewski, P.; Roozumek, M.; Aldinger, F. *J. Alloys Compounds* **2001**, *329*, 253−258.
(23) Britten, J. F. *Acta Crystallogr.* **1995**, *C51*, 1975−1977.
(24) Skakle, J. M. S.; Herd, R. *Powder Diffraction* **1999**, *14*, 195−203.
(25) Yamane, H.; Ogawara, K.; Omori, M.; Hirai, T. *J. Am. Ceram. Soc.* **1995**, *78*, 2385−2390.
(26) Taylor, D. *Trans. J. Br. Ceram. Soc.* **1984**, *83*, 92−98.
(27) Åhman, J.; Svensson, G.; Albertsson, J. *Acta Crystallogr.* **1996**, *C52*, 1336−1338.
(28) Kuncewicz-Kupczyk, W.; Kobertz, D.; Miller, M.; Chatillon, C.; Singheiser, L.; Hilpert, K. *J. Am. Ceram. Soc.* **2002**, *85*, 2299−2305.
(29) Kanke, Y.; Navrotsky, A. *J. Solid State Chem.* **1998**, *141*, 424−436.
(30) Chase, M. W., Jr., *NIST-JANAF Thermochemical Tables*, 4th ed.; The American Institute of Physics for The National Institute of Standards and Technology: New York, 1998.
(31) Shannon, R. D. *Acta Crystallogr.* **1976**, *A32*, 751−767.